TIME-DOMAIN ASTRONOMY

Enhanced x-ray emission coinciding with giant radio pulses from the Crab Pulsar

Teruaki Enoto[1]†*, Toshio Terasawa[2,3,4]†*, Shota Kisaka[5,6,7]†*, Chin-Ping Hu[1,8,9]†*, Sebastien Guillot[10], Natalia Lewandowska[11], Christian Malacaria[12,13], Paul S. Ray[14], Wynn C.G. Ho[11,15], Alice K. Harding[16,17], Takashi Okajima[16], Zaven Arzoumanian[16], Keith C. Gendreau[16], Zorawar Wadiasingh[16,18], Craig B. Markwardt[16], Yang Soong[16], Steve Kenyon[16], Slavko Bogdanov[19], Walid A. Majid[20,21], Tolga Güver[22], Gaurava K. Jaisawal[23], Rick Foster[24], Yasuhiro Murata[25,26,27], Hiroshi Takeuchi[25,27], Kazuhiro Takefuji[26,28], Mamoru Sekido[28], Yoshinori Yonekura[29], Hiroaki Misawa[30], Fuminori Tsuchiya[30], Takahiko Aoki[31], Munetoshi Tokumaru[32], Mareki Honma[33,34,35], Osamu Kameya[33,35], Tomoaki Oyama[33], Katsuaki Asano[2], Shinpei Shibata[36], Shuta J. Tanaka[37]

Giant radio pulses (GRPs) are sporadic bursts emitted by some pulsars that last a few microseconds and are hundreds to thousands of times brighter than regular pulses from these sources. The only GRP-associated emission outside of radio wavelengths is from the Crab Pulsar, where optical emission is enhanced by a few percentage points during GRPs. We observed the Crab Pulsar simultaneously at x-ray and radio wavelengths, finding enhancement of the x-ray emission by 3.8 ± 0.7% (a 5.4σ detection) coinciding with GRPs. This implies that the total emitted energy from GRPs is tens to hundreds of times higher than previously known. We discuss the implications for the pulsar emission mechanism and extragalactic fast radio bursts.

Spinning neutron stars emit periodic radio pulses from their magnetospheres, which can be observed as a pulsar. The radio pulses are emitted by a coherent mechanism (*1*). Some pulsars also show optical, x-ray, and gamma-ray pulses, which are usually interpreted using incoherent emission mechanisms. Giant radio pulses (GRPs) are a form of sporadic pulsar emission that have radio fluences at least an order of magnitude higher than those of regular pulses and are of unknown origin (*2*, *3*). GRPs have a power-law intensity distribution, unlike regular pulses, which have log-normal or exponential intensity distributions (*4*).

GRPs are bright, sometimes exceeding a megajansky (MJy, where 1 Jy = 10^{-26} W m^{-2} Hz^{-1}) for a few nanoseconds to microseconds (*5*). This is sufficient to detect each GRP during a single stellar rotation. GRPs from young neutron stars have been proposed as the origin of fast radio bursts (FRBs), short-duration radio transients at cosmological distances (*6*, *7*). A nearby counterpart has provided evidence for this association (*8*, *9*) and for a connection between coherent and incoherent processes in the neutron star magnetosphere (*10*). Although GRPs are not the leading explanation for FRBs, the broadband characteristics of GRPs provide information on coherent radio emission in neutron star magnetospheres that may be relevant to FRBs.

GRPs have been detected from only a small fraction of pulsars (*11*, *12*). The pulsar in the Crab Nebula, known as the Crab Pulsar (PSR B0531+21), was initially discovered by its GRPs (*13*). Regular periodic emission from the Crab Pulsar occurs from low-frequency radio waves to high-energy gamma rays. At 2 GHz (S-band), the GRP emission occurs at two rotational phases: the main pulse (MP) and the interpulse (IP), with a phase separation of 0.4 cycles. Sporadic GRPs occur both at the MP and IP of the average radio pulse, with each individual GRP lasting for a much narrower interval (~3 × 10^{-4} in phase) than the regular pulse.

Previous studies have searched for a correlation between radio giant pulses and higher energy emission [table S1; (*14*)]. The radio flux of GRPs is two to three orders of magnitude higher than regular pulses, and such a large enhancement does not occur at other wavelengths. An enhancement of ~3% (7.8σ significance) is known in the optical band (650 to 700 nm) (*15*) and has been independently confirmed (*16*). X-ray and gamma-ray observations have not detected any statistically significant correlations (*14*).

We searched for enhancement in x-rays during GRPs from the Crab Pulsar using the *Neutron star Interior Composition Explorer* (*NICER*) x-ray observatory mounted on the International Space Station (*17*). *NICER* has an effective collecting area of 1900 cm^2 at 1.5 keV, time resolution <100 ns, and flexible scheduling. Since launch in 2017, we have monitored the Crab Pulsar with *NICER* for calibration and scientific purposes. The total average count rate of the Crab Pulsar and Crab Nebula combined is 1.1 × 10^4 counts s^{-1} in the 0.3- to 10-keV band (~370 counts per spin cycle), which is below *NICER*'s maximum throughput of ~3.8 × 10^4 counts s^{-1}, and thus the data are nearly unaffected by pileup, dead-time, and data-transfer losses. The constant emission from the Crab Nebula (1.03 × 10^4 counts s^{-1}) was subtracted before analyzing the GRPs. We also observed the Crab Pulsar with two radio telescopes in Japan: the 34-m radio telescope of the Kashima Space Technology Center (*18*) and the 64-m radio dish of the Usuda Deep Space Center, both operating at 2 GHz [tables S2 to S5 and figs. S1 to S8; (*14*)]. In 2017–2019, we coordinated 15 *NICER* observations concurrently with either the Usuda or Kashima observatories [tables S2 and S6; (*14*)]. We extracted a total of 126 ks of exposure with simultaneous radio and x-ray coverage (*14*). The arrival time of

[1]Cluster for Pioneering Research, RIKEN, Wako 351-0198, Japan. [2]Institute for Cosmic Ray Research, University of Tokyo, Kashiwa 277-8582, Japan. [3]Mizusawa VLBI Observatory, National Astronomical Observatory of Japan, Mitaka 181-8588, Japan. [4]Interdisciplinary Theoretical Science Research Group, RIKEN, Wako 351-0198, Japan. [5]Frontier Research Institute for Interdisciplinary Sciences, Tohoku University, Sendai 980-8578, Japan. [6]Astronomical Institute, Tohoku University, Sendai 980-8578, Japan. [7]Department of Physical Science, Hiroshima University, Higashi-Hiroshima 739-8526, Japan. [8]Department of Physics, National Changhua University of Education, Changhua 50007, Taiwan. [9]Department of Astronomy, Kyoto University, Kyoto 606-8502, Japan. [10]Institut de Recherche en Astrophysique, Toulouse 31028, France. [11]Department of Physics and Astronomy, Haverford College, Haverford, PA 19041, USA. [12]NASA Marshall Space Flight Center, National Space Science and Technology Center, Huntsville, AL 35805, USA. [13]Universities Space Research Association, Science and Technology Institute, Huntsville, AL 35805, USA. [14]US Naval Research Laboratory, Washington, DC 20375, USA. [15]Mathematical Sciences and STAG Research Centre, University of Southampton, Southampton SO17 1BJ, UK. [16]NASA Goddard Space Flight Center, Greenbelt, MD 20771, USA. [17]Theoretical Division, Los Alamos National Laboratory, Los Alamos, NM 87545, USA. [18]Universities Space Research Association, Columbia, MD 21046, USA. [19]Columbia Astrophysics Laboratory, Columbia University, New York, NY 10027, USA. [20]Jet Propulsion Laboratory, California Institute of Technology, Pasadena, CA 91109, USA. [21]California Institute of Technology, Pasadena, CA 91125, USA. [22]Istanbul University, Science Faculty, Department of Astronomy and Space Sciences, Beyazıt, 34119 Istanbul, Turkey. [23]National Space Institute, Technical University of Denmark, Elektrovej 327-328, Denmark. [24]Massachusetts Institute of Technology Kavli Institute for Astrophysics and Space Research, Cambridge, MA 02139, USA. [25]Institute of Space and Astronautical Science, Japan Aerospace Exploration Agency, Sagamihara 252-5210, Japan. [26]Usuda Deep Space Center, Japan Aerospace Exploration Agency, Saku 384-0306, Japan. [27]Department of Space and Astronautical Science, SOKENDAI (The Graduate University for Advanced Studies), Sagamihara 252-5210, Japan. [28]Kashima Space Technology Center, National Institute of Information and Communications Technology, Kashima 314-8501, Japan. [29]Center for Astronomy, Ibaraki University, Mito 310-8512, Japan. [30]Planetary Plasma and Atmospheric Research Center, Tohoku University, Sendai 980-8578, Japan. [31]The Research Institute for Time Studies, Yamaguchi University, Yamaguchi 753-8511, Japan. [32]Institute for Space-Earth Environmental Research, Nagoya University, Nagoya 464-8601, Japan. [33]Mizusawa VLBI Observatory, National Astronomical Observatory of Japan, Oshu 023-0861, Japan. [34]Department of Astronomy, University of Tokyo, Tokyo 113-0033, Japan. [35]Department of Astronomical Science, SOKENDAI (The Graduate University for Advanced Studies), Mitaka 181-8588, Japan. [36]Department of Physics, Yamagata University, Yamagata 990-8560, Japan. [37]Department of Physics and Mathematics, Aoyama Gakuin University, Sagamihara 252-5258, Japan.

†These authors contributed equally to this work.

*Corresponding author. Email: teruaki.enoto@riken.jp (T.E.); terasawa@icrr.u-tokyo.ac.jp (T.T.); kisaka@hiroshima-u.ac.jp (S.K.); cphu0821@cc.ncue.edu.tw (C.-P. H.)

each x-ray photon was converted to barycentric dynamical time. Figure 1A shows the measured x-ray pulse profile in bins of 132 μs. The x-ray MP peak precedes the average radio profile by the rotation phase $\Delta\phi \cong 0.01$ (~300 μs), consistent with previous observations (*19*). Movie S1 shows how this profile accumulated as a function of exposure.

During the concurrent coverage, we detected ~2.49×10^4 and ~1.75×10^3 GRPs at the MP and IP phases of ϕ = 0.9917 to 1.0083 and ϕ = 1.3944 to 1.4111, respectively (hereafter MP-GRPs and IP-GRPs, respectively). The occurrence rates of MP-GRPs and IP-GRPs at the S-band are 0.67% (24,851 cycles) and 0.047% (1,749 cycles), respectively, of the observed 3,731,830 pulsar rotations. Figure 1A shows the phase distribution of the GRPs. We defined our GRP samples as those pulses with signal-to-noise ratio exceeding 5.0σ, which corresponds to a fluence of $\gtrsim 10^3$ Jy μs [fig. S8 (*14*)]. The occurrence phases and fractions of the MP- and IP-GRPs are consistent with past measurements (*20*, *21*).

We combined the x-ray photons in three bins, corresponding to pulsar rotation cycles where MP-GRPs, IP-GRPs, or neither occurred. These are hereafter referred to as MP-GRP-associated, IP-GRP-associated, or non-GRP-associated x-ray events, respectively. Figure 1B compares the MP-GRP-associated x-ray profile with the non-GRP-associated profile. The MP-GRP-associated x-ray profile shows an enhancement around the phase of the MP, with characteristics similar to those of the previously reported optical enhancement (*15*, *16*). Within the pulse phase interval ϕ = 0.985 to 0.997 [the same width as the optical measurement (*16*), taking into account the observed phase shift between the x-ray and optical bands (*22*)], the MP-GRP-associated x-ray profile shows an enhancement by 3.8±0.7% over the non-GRP-associated profile. We performed the same analysis for IP-GRP-associated x-rays, but did not find statistically significant enhancement, deriving a 3σ upper limit of 10% at ϕ = 1.378 to 1.402 rotational phase (*14*). Hereafter, we focus on the MP-GRP-associated case.

To evaluate the statistical significance of this enhancement, we generated synthetic x-ray samples that have no correlation with MP-GRPs, taking into account the look elsewhere effect (*23*). We randomly selected x-ray events with the same number of cycles as the MP-associated ones (24,826 cycles) from the non-GRP-associated sample. We repeatedly generated 1000 synthetic control samples and made a histogram of simulated enhancements (*14*). This histogram has a Gaussian distribution with mean −0.02% and SD 0.70%. Therefore, the significance of our measured enhancement is 3.8%/0.70% = 5.4σ. Figure 2 shows the growth curves of the detection significance and the x-ray enhancement rate as a function of the accumulated numbers of MP-GRP-associated cycles. The curves show the expected monotonic increase in significance, proportional to the square root of the number of the MP-GRP-associated cycles, and a consistent x-ray enhancement rate. We also confirmed this detection with a lag analysis (*14*). We did not detect any spectral changes (at the MP)

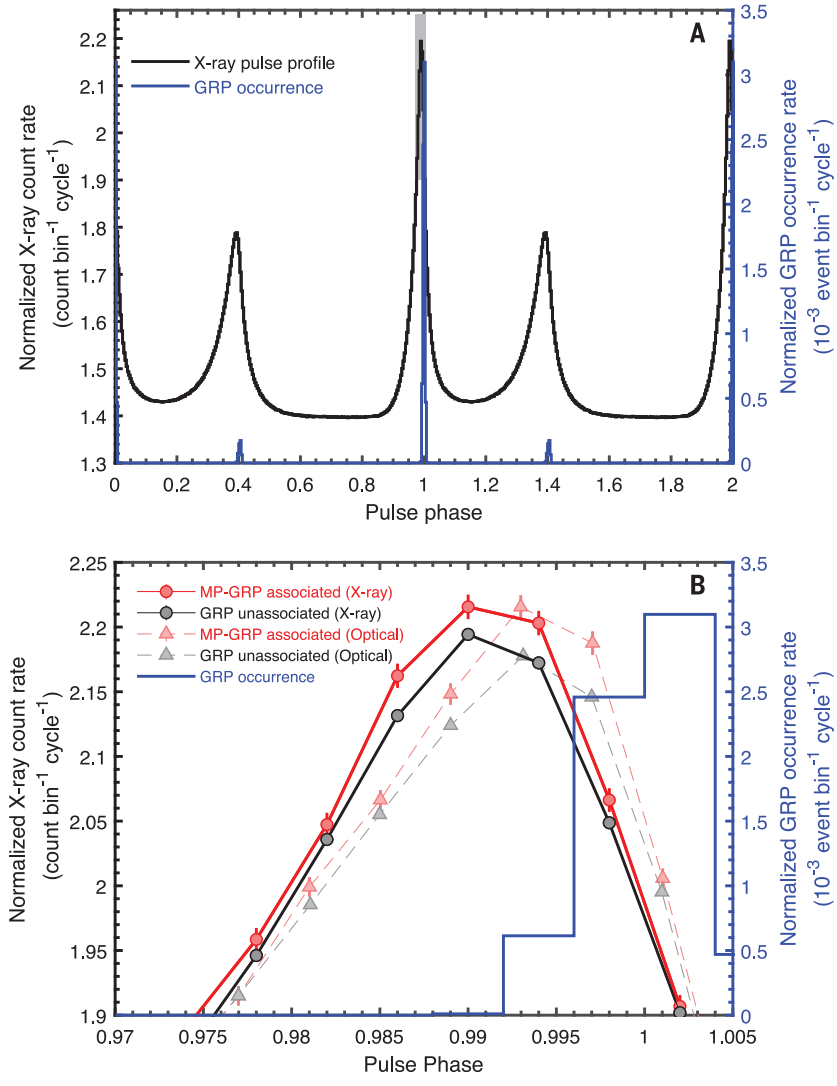

Fig. 1. X-ray and optical pulse profiles of the Crab Pulsar compared with GRPs. (**A**) The 0.3- to 10.0-keV profile (black histogram) observed with *NICER* in 2017–2019 (left axis). The profile was generated with 250 phase bins per spin period, includes the contribution from the Crab Nebula, and is normalized by the total number of pulsar spin cycles. Two pulse cycles are shown for clarity. The phase distribution of GRPs is shown in blue, as measured in our 2.2- to 2.3-GHz radio data from the Usuda and Kashima observatories (right axis). (**B**) A zoomed view of gray-shaded area of (A). Black and red circle symbols connected with solid lines show the x-ray profiles without and with GRP association, respectively, with error bars indicating the 1σ statistical uncertainties (error bars of the black circle and gray triangle points are too small to be visible). The blue histogram shows the GRP occurrence distribution [identical to (A)]. The faint dashed lines (black and red triangle symbols) show the optical profiles without and with GRP association, respectively, normalized by an arbitrary scaling (*16*).

between the GRP-associated and the non-GRP-associated profiles, only an increase in normalization corresponding to the GRP enhancement (*14*).

The total number of x-ray photons concurrent with radio observations in our analysis was 1.4×10^9 counts, about three orders of magnitude higher than previous x-ray studies [e.g., (*3*, *21*)]. Figure 3 compares our detection of the x-ray enhancement of MP-GRPs with previous multiwavelength studies [table S1; (*14*)]. Our detection of a 3.8% x-ray enhancement is consistent with the upper limits of ~10% obtained in previous studies and similar to the measured 3.2 ± 0.5% optical enhancement (*16*). The pulse phase where this x-ray excess appears, ϕ = 0.985 to 0.997, is also consistent with the reported enhancement phase (ϕ = 0.987 to 0.999) at optical wavelengths (*16*). This implies that the MP-GRP-associated higher-energy component extends from optical to x-rays without a change in the pulse phase or a spectral cutoff compared with the average regular pulse. The x-ray flux of the regular pulsed emission ($\sim 4.43 \times 10^{-9}$ ergs s^{-1} cm^{-2} in 0.3 to 10 keV) is ~1000 and ~10^7 times higher than those of the optical pulses [$\sim 4.6 \times 10^{-12}$ ergs s^{-1} cm^{-2} at 5500 Å (*24*)] and regular radio pulses [$\sim 1.7 \times 10^{-16}$ ergs s^{-1} cm^{-2} at 2 GHz (*25*)], respectively. Assuming the same enhancement rate (~4%) in both the optical and x-ray bands implies one to two orders of magnitude higher total energy (both flux and fluence) emitted from GRP-associated events than the value derived from the radio and optical data only.

If the x-ray enhancement derived by averaging over ~300 μs (Fig. 1) consists of multiple short pulses similar to GRP pulses (a typical duration of ~15 μs for each GRP, evaluated as fluence divided by the individual peak flux), the peak x-ray flux could be much higher (~20 times) than the averaged enhancement flux.

These results constrain the GRP emission mechanism. The same degree of enhancements (~4%) between the optical and x-rays indicates that the GRP-associated high-energy radiation has the same spectral energy distribution as that of regular pulses. Thus, the energy distribution of GRP-emitting particles is similar to those of particles emitting regular pulses, which result from particle acceleration in the pulsar magnetosphere or a thin corrugated plasma flow at the equatorial plane (a current sheet). The x-ray emission associated with GRPs implies that the radio emission efficiency is ≲1%, consistent with a magnetic reconnection model (*26*).

A previously proposed model of GRP high-energy radiation invokes a temporal increase in particle number density in the emitting region (*27*). The difference in enhancement between the radio (several orders of magnitude) and optical/x-ray bands (~4%) is then attributed to incoherent (x-ray and optical) emissions being proportional to the particle number, whereas coherent (radio) emission is proportional to the particle number squared (see the supplementary text). Other proposed mechanisms are emission from high-energy particles in the plasma blobs (plasmoids) generated by magnetic reconnection (*26*) or from the resonant absorption of radio photons by x-ray emitting particles (*28*) (*14*).

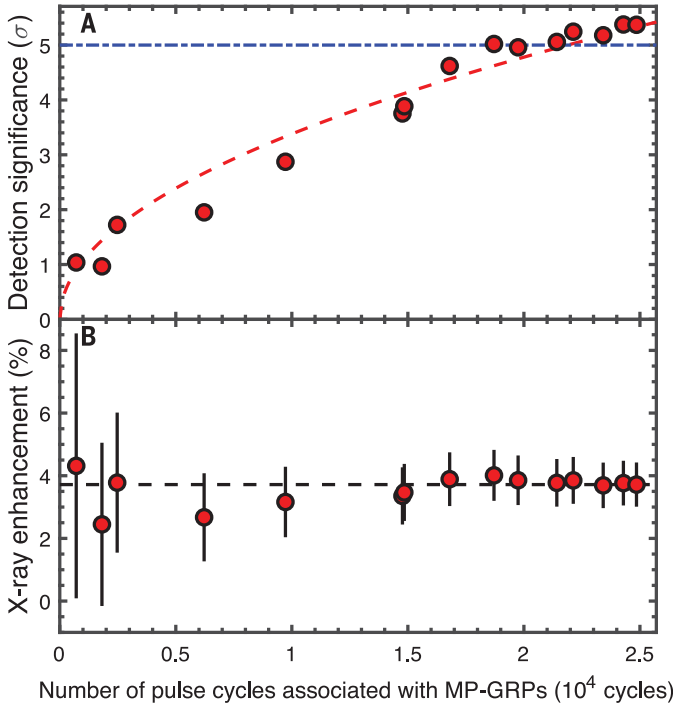

Fig. 2. Growth curves of the detection significance and x-ray enhancement. (**A**) Detection significance as a function of the accumulated number of rotation cycles observed to be associated with MP-GRPs. Data accumulation was performed chronologically, i.e., each data point represents all the *NICER* data up to that epoch. The horizontal blue dot-dashed line is the 5σ detection significance level, and the red dashed curve is the best-fitting model: the square root of the cycle number. (**B**) Same as (A) but for the degree of x-ray enhancement. The horizontal dashed line shows the 3.8% enhancement ratio derived from the entire dataset. Error bars are statistical 1σ uncertainties.

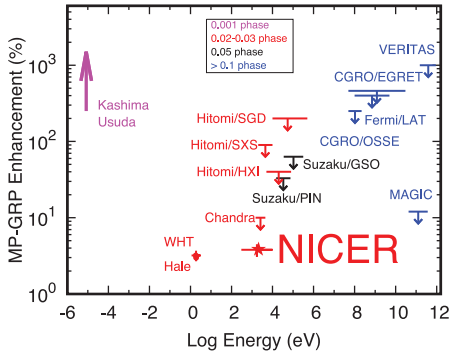

Fig. 3. Enhancement rates with MP-GRPs as a function of photon energy. Optical (WHT and Hale telescopes) and *NICER* data points are detections. All other observations are upper limits in the x-ray and gamma-ray bands indicated by downward arrows [values and references are listed in table S1, and abbreviations are defined in (14)]. Magenta, red, blue, and black colors represent different analyzed phase ranges of 0.001, 0.02 to 0.03, 0.05, and >0.1, respectively. For our observed radio enhancements with Kashima and Usuda, the detection threshold is shown with the magenta upward arrow.

Bright GRPs from young and energetic pulsars or magnetars have been proposed as low-energy analogs of FRBs (*7*), but this proposal has been disputed (*29*). The proposal relies on the unknown GRP radio emission efficiency η relative to the spin-down luminosity. Even in the case of an extremely high efficiency (η ~ 1), the spin-down time scale for FRB sources are shorter than 100 years (*29*, *30*). If FRBs are accompanied by x-ray emission increases similar to Crab GRPs, then the spin-down rate would be enhanced by a factor of 1/η with η << 1. This would cause rapid radio flux decay, which is inconsistent with observations of the repeating FRB 121102 (*31*). Our results therefore disfavor the proposed connection between GRPs and repeating FRBs.

REFERENCES AND NOTES

1. D. B. Melrose, R. Yuen, *J. Plasma Phys.* **82**, 635820202 (2016).
2. H. S. Knight, M. Bailes, R. N. Manchester, S. M. Ord, B. A. Jacoby, *Astrophys. J.* **640**, 941–949 (2006).
3. A. V. Bilous, M. A. McLaughlin, V. I. Kondratiev, S. M. Ransom, *Astrophys. J.* **749**, 24 (2012).
4. W. A. Majid, C. J. Naudet, S. T. Lowe, T. B. H. Kuiper, *Astrophys. J.* **741**, 53 (2011).
5. T. H. Hankins, J. A. Eilek, *Astrophys. J.* **670**, 693–701 (2007).
6. D. R. Lorimer, M. Bailes, M. A. McLaughlin, D. J. Narkevic, F. Crawford, *Science* **318**, 777–780 (2007).
7. J. M. Cordes, I. Wasserman, *Mon. Not. R. Astron. Soc.* **457**, 232–257 (2016).
8. C. D. Bochenek *et al.*, *Nature* **587**, 59–62 (2020).
9. CHIME/FRB Collaboration, *Nature* **587**, 54–58 (2020).

10. W. Lu, P. Kumar, B. Zhang, *Mon. Not. R. Astron. Soc.* **498**, 1397–1405 (2020).
11. R. N. Manchester, G. B. Hobbs, A. Teoh, M. Hobbs, *Astron. J.* **129**, 1993–2006 (2005).
12. T. Enoto, S. Kisaka, S. Shibata, *Rep. Prog. Phys.* **82**, 106901 (2019).
13. D. H. Staelin, E. C. Reifenstein 3rd, *Science* **162**, 1481–1483 (1968).
14. Materials and methods are available as supplementary materials.
15. A. Shearer *et al*., *Science* **301**, 493–495 (2003).
16. M. J. Strader *et al*., *Astrophys. J.* **779**, L12 (2013).
17. K. C. Gendreau *et al*., "The Neutron Star Interior Composition Explorer (NICER): design and development," in *Space Telescopes and Instrumentation 2016: Ultraviolet to Gamma Ray*, J.-W. den Herder, T. Takahashi, M. Bautz, Eds. (SPIE, 2016), vol. 9905 of *Proceedings of SPIE*, p. 99051H.
18. K. Takefuji *et al*., *Publ. Astron. Soc. Pac.* **128**, 084502 (2016).
19. A. Martin-Carrillo *et al*., *Astron. Astrophys.* **545**, A126 (2012).
20. R. Mikami *et al*., *Astrophys. J.* **832**, 212 (2016).
21. Hitomi Collaboration, *Publ Astron Soc Jpn Nihon Tenmon Gakkai* **70**, (2018).
22. R. Bühler, R. Blandford, *Rep. Prog. Phys.* **77**, 066901 (2014).
23. E. Gross, O. Vitells, *Eur. Phys. J. C* **70**, 525–530 (2010).
24. A. A. Abdo *et al*., *Astrophys. J.* **208**, 17 (2013).
25. A. V. Bilous *et al*., *Astron. Astrophys.* **591**, A134 (2016).
26. A. Philippov, D. A. Uzdensky, A. Spitkovsky, B. Cerutti, *Astrophys. J.* **876**, L6 (2019).
27. M. Lyutikov, *Mon. Not. R. Astron. Soc.* **381**, 1190–1196 (2007).
28. A. K. Harding, J. V. Stern, J. Dyks, M. Frackowiak, *Astrophys. J.* **680**, 1378–1393 (2008).
29. M. Lyutikov, *Astrophys. J.* **838**, L13 (2017).
30. S. Kisaka, T. Enoto, S. Shibata, *Publ. Astron. Soc. Jpn.* **69**, L9 (2017).
31. M. Cruces *et al*., *Mon. Not. R. Astron. Soc.* **500**, 448–463 (2021).
32. C. P. Hu, Source code and GRP list for Crab GRP analysis, Version 0.1, Zenodo (2021); https://doi.org/10.5281/zenodo.4586922.

ACKNOWLEDGMENTS

We thank Y. Terada and N. Kawai for suggestions on our analysis and manuscript; the Usuda 64-m antenna operation support team in Space Tracking and Communication Center and ISAS, JAXA for coordinating simultaneous observations with NICER; and E. Kawai and S. Hasegawa of the Space Time Standard Laboratory of the Kashima Space Technology Center of the National Institute of Information and Communications Technology (NICT) for supporting observations with the Kashima 34-m antenna. *NICER* analysis software and data calibration were provided by the NASA *NICER* mission and the Astrophysics Explorers Program. **Funding:** T.E., T.T., H.M., K.A., M.H., S.S., S.J.T., and S.K. are supported by JSPS/MEXT KAKENHI grant nos. 15H00845, 15K05069,16H02198, 17H01116, 17K18270, 17K18776, 18H01245, 18H01246, 18H04584, and 19K14712. T.E. acknowledges Hakubi projects of Kyoto University and RIKEN. W.C.G.H. acknowledges support through grant no. 80NSSC20K0278 from NASA. C.H. was supported as the JSPS International Research Fellow (ID: P18318) and by the Ministry of Science and Technology in Taiwan through grant no. MOST 109-2112-M-018-009-MY3. C.M. is supported by an appointment to the NASA Postdoctoral Program at the Marshall Space Flight Center, administered by Universities Space Research Association under contract with NASA. H.T. was supported by the discretionary expenses of the director of Institute of Space and Astronautical Science (ISAS), JAXA. W.A.M performed research at the Jet Propulsion Laboratory, California Institute of Technology, under a contract with the NASA. **Author contributions:** T.E. and T.T. led this radio-x-ray collaboration. T.T. and C.H. led the radio and x-ray timing analyses, respectively. S.G. performed the x-ray spectral analyses. S.K. led the theoretical discussion. P.S.R., T.O., Z.A., K.C.G., C.B.M., Y.S., S.K., S.B., and R.F. were responsible for *NICER* detector development, timing calibration, and observation planning. C.M., W.C.G.H., A.K.H., Z.W., W.A.M., T.G., G.K.J., K.A., S.S., N.L., and S.J.T. contributed to the theoretical interpretation. Y.M., H.T., K.T., M.S., Y.Y., H.M., F.T., T.A., M.T., M.H., O.K., and T.O. were responsible for the radio observations and associated data analyses. N.L. contributed the summary of previous studies. **Competing interests:** The authors declare no competing interests. **Data and materials availability:** The *NICER* x-ray data are available from the NASA HEASARC archive https://heasarc.gsfc.nasa.gov/ under the observation IDs listed in table S6. The HEASOFT x-ray analysis software is available from https://heasarc.gsfc.nasa.gov/docs/software/heasoft/. The GRP event lists and our analysis source codes are available on Zenodo (*32*).

SUPPLEMENTARY MATERIALS

science.sciencemag.org/content/372/6538/187/suppl/DC1
Materials and Methods
Supplementary Text
Figs. S1 to S20
Tables S1 to S7
References (*33*–*78*)
Movie S1

23 June 2020; accepted 5 March 2021
10.1126/science.abd4659